^{87}Rb NMR spectra of hydrogen-bonded $Rb_3D(SO_4)_2$ and $Rb_3H(SO_4)_2$ crystals

A. Titze, A. Maiazza,* G. Hinze, and R. Böhmer
Institut für Physikalische Chemie, Johannes-Gutenberg-Universität, D-55099 Mainz, Germany
(Received 18 August 1998)

The paraelectric and antiferroelectric phases of $Rb_3D(SO_4)_2$ and $Rb_3H(SO_4)_2$ were investigated using rubidium NMR. The angle dependence of the second order quadrupole shifted central ^{87}Rb transitions was recorded at 300 K. It was found to be in full agreement with the symmetry elements of a monoclinic $A2/a$ structure. The temperature dependence of the magnitude and asymmetry of the electrical field gradient (EFG) tensors at the Rb sites was determined using powder samples and revealed no differences between protonated and deuterated specimens. The antiferroelectric transition of $Rb_3D(SO_4)_2$ ($T_N = 82$ K) is associated with a quadrupling of the unit cell. Below T_N the magnitudes of the EFG at the Rb sites remain constant and smoothly tilt away from their high temperature orientations. The temperature dependence of the NMR line splittings associated with this tilt follows a power law implying an order parameter critical exponent of 0.21. [S0163-1829(99)07517-7]

I. INTRODUCTION

The phase transitions of hydrogen bonded solids usually exhibit an isotope effect. The melting point of deuterated ice (at 3.8 °C) provides a well known example. Also for ferroelectric and antiferroelectric crystals isotope effects are known and have been the subject of experimental and theoretical studies for a long time.[1,2] Particularly interesting in this respect are crystals of the $M_3D(XO_4)_2$ family with $M = \{Rb,K\}$ and $X = \{Se,S\}$. For these crystals the substitution of the deuterons by protons can lead to a complete suppression of electric order. Such a pronounced isotope effect has, e.g., been reported for $Rb_3H_{1-x}D_x(SO_4)_2$. Here, the fully deuterated compound exhibits a paraelectric↔antiferroelectric phase transition at $T_N = 82$ K.[10] Upon proton substitution T_N decreases and for $x < 0.22$ the paraelectric phase is stable down to the lowest temperatures.[3]

As for other hydrogen bonded crystals there is a debate[4] whether the isotope effect is purely geometrical[5] or predominantly quantum mechanical in nature.[6,7] In the framework of one of the theories aiming at understanding how hydrogen bonded crystals are driven into electrically ordered phases it has been argued that a coupling of phonon and tunneling modes should lead to ''self-trapped proton states'' [8] and consequently to asymmetric hydrogen bonds already in the paraelectric phase. A recent nuclear magnetic resonance (NMR) study of $Rb_3H(SO_4)_2$ powders has been interpreted to indicate that in this crystal the nonordered hydrogen bonds are asymmetric.[9]

In continuation of our previous work[10] in the present paper we report on ^{87}Rb NMR measurements that we have carried out for single crystals and powders of $Rb_3H_{1-x}D_x(SO_4)_2$ with $x = 0$ and $x = 1$. At room temperature these compounds exhibit the monoclinic $A2/a$ structure with $Z = 4$ formula units in the unit cell.[11] Sketches of the crystal structure as projected along the monoclinic b axis and along the a axis are shown in Fig. 1. The structure is characterized by sulfate tetrahedra which are linked to dimers via hydrogen bonds. When viewed along the monoclinic b axis these $[(SO_4)\cdot H\cdots(SO_4)]^{3-}$ ions are separated by Rb ions. Out of the twelve Rb ions per unit cell four symmetric units [denoted Rb(1)] together with the centers of the hydrogen bonds are located in the a-b plane. The other eight crystallographically equivalent Rb(2) sites separate the planes of sulfate dimers when seen along the c^* axis. As indicated in Fig. 1 we define the c^* axis to be normal to the a-b plane. For our NMR investigations it is important to note that while all Rb(1) sites are connected via inversion symmetry there are two groups of Rb(2) sites denoted as Rb(2′) and Rb(2″).

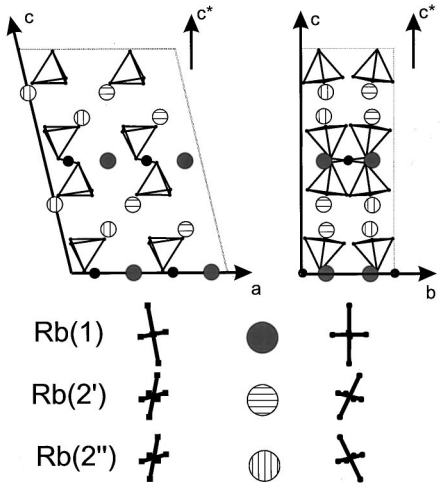

FIG. 1. Sketch of projections along the crystallographic b axis (left-hand side) and the a axis (right-hand side) of the paraelectric $A2/a$ ($Z = 4$) structure of $Rb_3D(SO_4)_2$. Upper part: Paraelectric crystal structure. The sulfate tetrahedra are linked via hydrogen bonds (straight lines). The deuterons are depicted as dots located (on the time average) in the center of the hydrogen bonds. The dimers are separated in the c^* direction (defined to be normal to the a-b plane) by rubidium atoms [Rb(2) sites]. Lower part: Projections of the EFG tensors for the different Rb sites. The tensors of Rb(2′) and Rb(2″) can be transformed into one another by a glide reflection along the a-c plane. The assignment as 2′ and 2″ chosen for representation in this figure is arbitrary.

The four Rb(2″) sites are obtained from the four Rb(2′) sites by a glide reflection.

This article is organized as follows. In the next section we will present the framework required to analyze quadrupole perturbed NMR spectra. Section III gives the experimental details. In Sec. IV we present the orientation and temperature dependence of the absorption spectra of single crystals and powders as taken in a large temperature range. We summarize in Sec. V.

II. THEORETICAL CONSIDERATIONS

One of the goals of the present work is to determine the electrical field gradient (EFG) tensor $V_{\alpha\beta}$ of the ^{87}Rb probe from its second-order shifted central transition spectra.[12] The frequency shift $\nu-\nu_L$ with respect to the Larmor frequency ν_L depends on the angle enclosed by the external magnetic field (taken to be oriented along the *z*-axis) and the principal axes of the EFG tensor. Using $V_{\alpha\beta}=\partial^2 V/\partial\alpha\,\partial\beta$, with $\alpha,\beta=\{x,y,z\}$ and V denoting the electrical potential in the laboratory axis system (LAS) one has[13,14]

$$\nu-\nu_L=K[2(V_{xz}^2+V_{yz}^2)-(V_{xx}-V_{yy})^2/4-V_{xy}^2]. \quad (1)$$

Here $K=-\nu_Q^2/(3\nu_L V_{ZZ}^2)$ determines the quadrupolar coupling with $\nu_Q=eQV_{ZZ}/2h$ and $V_{ZZ}=eq$ denoting the largest eigenvalue of the EFG in the principal axis system (PAS). These tensor elements were determined by rotating the sample around three orthogonal crystal axes and recording the positions of the resonance frequencies. If θ denotes the rotation angle around the *x* axis, say, in the LAS then Eq. (1) can be expressed in terms of five Fourier components d_0, d_1, d_2, d_3, and d_4 as[14]

$$\nu-\nu_L=K[d_0+d_1\sin(2\theta)+d_2\cos(2\theta)+d_3\sin(4\theta)+d_4\cos(4\theta)]/32. \quad (2)$$

Only the coefficients $d_3=-36(V_{yy}-V_{zz})V_{yz}$ and $d_4=-9(V_{yy}-V_{zz})^2+36V_{yz}$ as well as those obtained from rotations around two other orthogonal axes are used in the determination of the EFG tensors. From a diagonalization of $V_{\alpha\beta}$ the principal values of the EFG tensor, i.e., V_{XX}, V_{YY}, and V_{ZZ}, as well as the orientation of the PAS with respect to the LAS were obtained. From this information we have determined the quadrupolar coupling constant ν_Q, the asymmetry parameter $\eta=(V_{XX}-V_{YY})/V_{ZZ}$, and the three Euler angles specifying the transformation between LAS and PAS.

Structural changes in crystals are associated with the displacement of ionic charges and thus with a modification of the EFG tensor. In a simple point charge model the contribution of a charge e at $\mathbf{r}=(r_x,r_y,r_z)$ to the EFG can easily be calculated. If the EFG tensor is located at the origin of the coordinate system then one has[15] $V_{\alpha\beta}=e(3r_\alpha r_\beta-\delta_{\alpha\beta}r^2)/r^5$ with $r=|\mathbf{r}|$. The total EFG tensor is then obtained by summing over all charges. If $\mathbf{r}$ changes slightly, e.g., due to thermal contraction, then the relative variation of the tensor element is $\Delta V_{\alpha\beta}/V_{\alpha\beta}=-3\Delta r/r$. The change of the second order line shift $\delta\nu\equiv\nu(\{V_{\alpha\beta}\})-\nu(\{V'_{\alpha\beta}\})$ can be calculated using Eq. (1). Inserting $V'_{\alpha\beta}=V_{\alpha\beta}+\Delta V_{\alpha\beta}$ into this equation to lowest order yields

$$\delta\nu=-2K[2(V_{xz}\Delta V_{xz}+V_{yz}\Delta V_{yx})-(V_{xx}-V_{yy})(\Delta V_{xx}-\Delta V_{yy})/4-V_{xy}\Delta V_{xy}]. \quad (3)$$

Thus the line shift is proportional to small variations in the EFG-tensor elements which in turn are proportional to small changes in the distances between the probe nucleus and the ions in its vicinity.

Sometimes only the determination of the quadrupolar coupling constant and the asymmetry of an EFG tensor but not its orientation is of interest. Then it suffices to measure spectra of *powdered* samples. For a quantitative analysis of the powder spectra presented in this article we have performed numerical simulations. To this end we have added the frequency contributions [as calculated according to Eq. (1)] from a large ensemble of EFG tensors with randomly oriented principal axes. In order to obtain overall isotropic, sufficiently ''noise-free'' simulated spectra the contributions from about 10^5 ''grains'' were added. We have checked for a number of parameters ν_Q and η that the powder spectra thus obtained agree with those calculated from analytical expressions.[16] In order to determine ν_Q and η from the experimental data we have implemented this simulation procedure into a least-squares fitting routine. To account for a finite dipolar broadening the simulated spectra were convoluted with a relatively narrow Gaussian or Lorentzian line (typical width 1 kHz).

III. EXPERIMENTAL DETAILS

$Rb_3D(SO_4)_2$ crystals of optical quality were grown from aqueous solutions of Rb_2SO_4 and D_2O with an excess of D_2SO_4. Analogously for the protonated compound H_2O and H_2SO_4 were used. The solutions were placed in closed vessels on a heated surface ($T\approx 70\,^\circ$C) for several days and crystals were grown by a convection method. Quasihexagonally shaped platelets with a size of typically $5\times2\times10\,\mathrm{mm}^3$ were obtained. For some of the NMR measurements finely powdered samples with a grain size of a few μm were used.

Several experimental methods were employed to characterize the crystals. From polarization microscopy no signs for twinning could be observed in our samples. Studies using a two-axis goniometer revealed that particularly the (001), $(00\bar{1})$, (312), and $(1\bar{1}2)$ faces were well established. X-ray measurements carried out at room temperature confirmed the monoclinic space group $A2/a(Z=4)$. The lattice parameters were found to be $a=10.2$ Å, $b=6.0$ Å, $c=15.0$ Å, and $\beta=103.1^\circ$ at room temperature; see also Ref. 11. The paraelectric to antiferroelectric phase transition of $Rb_3D(SO_4)_2$ was observed with dielectric measurements. From the frequency independent maximum of the dielectric constant we find a transition temperature of $T_N=82$ K.

The NMR measurements were performed utilizing a home-built spectrometer. For our studies we used the quadrupole perturbed central transition ($1/2\rightarrow-1/2$) of the ^{87}Rb ($I=3/2$) nuclear probe at a Larmor frequency of about $\nu_L=85.7$ MHz. Frequency offsets $\nu-\nu_L$ are given with respect to a solution of RbCl in D_2O. Absorption spectra were obtained with standard solid echo sequences employing 90° pulse lengths of typically 2 μs. However, in order to record

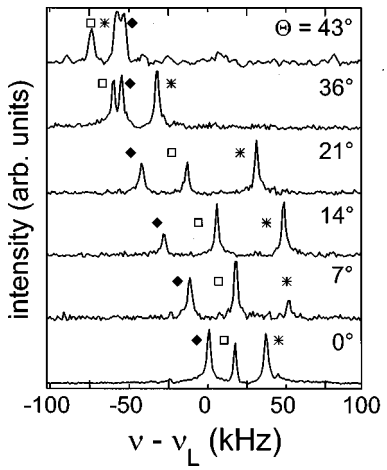

FIG. 2. Typical spectra of the central transitions of $Rb_3D(SO_4)_2$ at room temperature. No efforts were made to achieve a uniform excitation of all three resonances. Therefore the three equally strong lines here appear with different intensities. The resonance positions are summarized in the lower frame of Fig. 3. The Rb(1) peaks are marked by the stars. The other symbols refer to the Rb(2) sites.

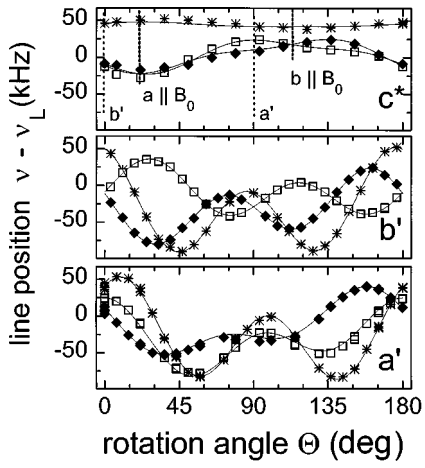

FIG. 3. Angular positions of the resonance positions recorded by rotating a $Rb_3D(SO_4)_2$ single crystal around an axis perpendicular to the external magnetic field. From top to bottom the three frames correspond to rotations around the c^*, the b', and the a' axes of the crystal. The orientations marked b' and a' in the upper frame correspond to the $\Theta = 0°$ positions in the middle and lower frame, respectively. The positions where the a and b axes are parallel to the external magnetic field are also indicated. They enclose an angle of 25° with the primed axes. The solid lines represent fits using Eq. (2) and yielded the EFG tensors schematically represented in Fig. 1 (see also Table I). The symbols have the same meaning as in Fig. 2.

the angle dependence of the resonance frequencies, the so-called rotation pattern, larger coils, and consequently longer pulses (10 μs) were necessary. For the determination of the rotation patterns, we utilized a sample holder which allowed mounting of the specimen in three mutually orthogonal positions. In each of these positions the sample holder could be rotated around an axis perpendicular to the external magnetic field. The precision achieved for the angular adjustment was better than 1°. Temperatures were measured from calibrated Ir sensors which are accurate to within ± 0.5 K. Stability during one measurement typically was ± 0.1 K.

IV. RESULTS AND DISCUSSION

A. Symmetry of the EFG at room temperature

In Fig. 2 we present single crystal spectra of $Rb_3D(SO_4)_2$ recorded at room temperature. It is seen that the position of the three resonance lines shifts upon rotating the crystal. For these experiments large coils (and long radiofrequency pulses) were used. The large coils permitted rotation of the crystal, but did not allow a uniform excitation across the entire spectral range. However, from experiments employing shorter pulses we know that the lines exhibit equal intensities when suitably irradiated. Since the unit cell of $Rb_3D(SO_4)_2$ contains twelve Rb ions, each line corresponds to four sites in that cell.

In order to achieve a structural assignment of the lines we rotated the crystal around three mutually orthogonal axes. The results of this procedure are collected in Fig. 3. The rotation around the c^* axis (which is perpendicular to the a-b plane) is particularly instructive. The rotation induced changes in the second order shifts are small as compared to those around the two other axes. This implies that the largest principal axes of the EFG tensors are not tilted far from the c^* axis. For a quantitative analysis of these rotation patterns, we have used Eq. (2). From the coefficients d_3 and d_4 we have determined the quadrupolar coupling constants ν_Q and the asymmetry parameters η as well as the orientations of the EFG tensors in the system of crystal axes for all three sites.

Our findings are summarized in Table I. It turns out that two of the sites show the same ν_Q and η values. Furthermore one set of Euler angles characterizing the orientation of the EFG tensor, within experimental uncertainty, can be obtained from the other by inversion. These findings imply the existence of a plane of reflection or glide reflection. Therefore these sites are unambiguously recognized as the Rb(2) sites. For the remaining EFG tensor, one principal axis points along the twofold monoclinic axis as required by the symmetry of the $A2/a$ phase. Thus the orientations of the EFG tensors, which are sketched in the lower part of Fig. 1, are in full agreement with the crystallographic symmetry.[17]

TABLE I. EFG tensor parameters characterizing the three rubidium sites. The Euler angles describe how the crystallographic axes a, b, and c^* are transformed into the principal axes system of the EFG tensor. We used the standard definition with φ being the rotation angle around c^*, χ that around the new b axis, and ψ denoting the rotation angle around the finally obtained c^* axis. Within experimental error ($\approx 1°$) one principal axis of the EFG tensor at the Rb(1) site points along the twofold monoclinic axis as required by symmetry. The existence of a reflection (glide) plane is borne out by the Euler angles of Rb(2′) with respect to those characterizing Rb(2″).

Site	Rb(1)	Rb(2′)	Rb(2″)
ν_Q (MHz)	4.8	3.8	3.8
η	0	0.45	0.45
φ (deg)	0	67	−67
χ (deg)	10	28	27
ψ (deg)	0	−113	115

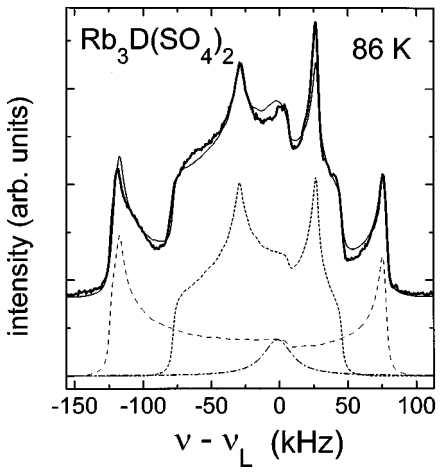

FIG. 4. A typical spectrum of a powdered sample (thick solid line) taken at 86 K. The thin solid line is the result of the simulation procedure described in the text. The dashed and dotted lines show the contributions for the Rb(1) and Rb(2) sites, respectively.

The quadrupolar coupling constants and asymmetry parameters are found to be $\nu_Q = 4.8$ MHz and $\eta = 0$ for Rb(1) and $\nu_Q = 3.85$ MHz and $\eta = 0.45$ for Rb(2); see Table I. We note that these parameters are substantially different from those determined in a previous Rb-NMR investigation of powdered $Rb_3H(SO_4)_2$ samples.[9] The observation in Ref. 9 is surprising in view of the fact that we were able to determine ν and η from powder spectra very reliably. This will be documented in the following.

B. Temperature dependent coupling constants

A representative powder spectrum of $Rb_3D(SO_4)_2$ is shown in Fig. 4. The lower part of this figure reveals that this spectrum can be decomposed into several distinct contributions. One contribution is due to an axially symmetric EFG tensor as is immediately recognized from the singularities located on the outer edges of the spectrum.[16] This part of the spectrum obviously is due to the Rb(1) site. Then there is a second nonaxially symmetric contribution from the Rb(2) site which exhibits an integrated area twice that of the former. This intensity ratio was to be expected since in powdered samples symmetry equivalent, but differently oriented, EFG tensors can of course not be distinguished. In addition to these features, there is a weaker central component which is not anticipated from the single crystal spectra. After most of the powder spectra reported in this article were collected we found out that the intensity of the central component could be affected by subjecting these samples to elevated temperatures. Therefore we suspect that moisture at the grain surfaces gives rise to the central feature.

Figure 5(a) shows powder spectra of $Rb_3D(SO_4)_2$ as measured for several temperatures. It is seen that upon cooling the splitting of the outer edge singularities of the axially symmetric EFG tensor at first increases but then below about 80 K saturates.[18] The shape of the central component which is due to the Rb(2) site does not change much with temperature. In order to determine the quadrupole coupling constants and the asymmetry parameters from these spectra we have used the simulation procedure described in Sec. II taking also into account the central component. The thin solid line in Fig. 4 which is a fit result shows that the simulation technique provides a good description of the spectra. The temperature dependent quadrupole coupling constants determined from least-squares fits are summarized in Fig. 6. It is seen that at room temperature where direct comparison with single crystal parameters is possible the powder data nicely reproduce ν_Q as given in Table I. The same is true for the asymmetry parameters. We find $\eta = 0.43 \pm 0.02$ for the Rb(2) site and $\eta = (0.02 \pm 0.03)$ for the Rb(1) site, independent of temperature.

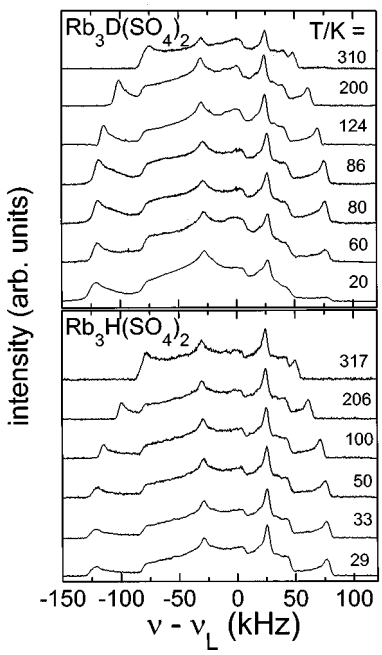

FIG. 5. Temperature dependent powder spectra of the deuterated (upper frame) and protonated samples (lower frame). Only the outer peaks exhibit a pronounced temperature shift. Below about 80 K the line splitting remains constant.

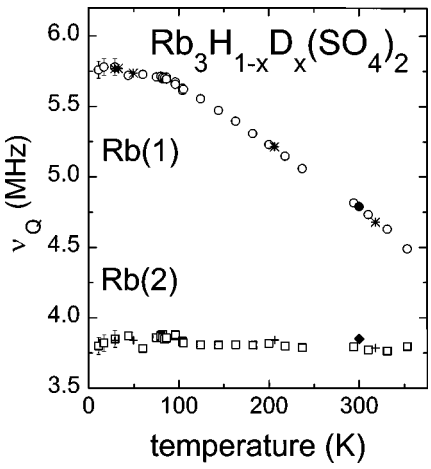

FIG. 6. Temperature dependent quadrupolar coupling constants ν_Q of the protonated (*,+) and the deuterated (○,□) samples. The coupling constants were determined from powder spectra (open symbols) or single crystal rotation patterns (filled symbols). ν_Q is independent of the degree of deuteration. Below the paraelectric to antiferroelectric phase transition the quadrupolar couplings are constant within experimental uncertainty.

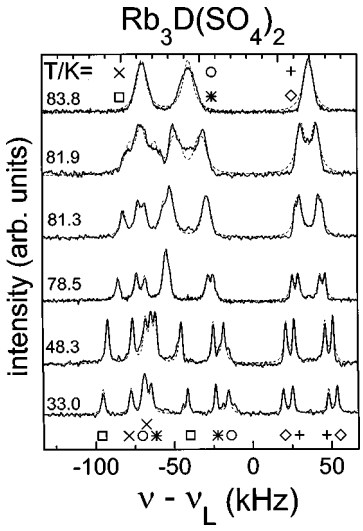

FIG. 7. Temperature dependent single crystal spectra of $Rb_3D(SO_4)_2$ as measured near and below the phase transition. A crystal orientation was chosen that exhibits a large separation of lines in the paraelectric phase. The lines quadruple as the crystal is cooled through the phase transition. The spectra can be fitted with a superposition of twelve Gaussian profiles for each temperature (dotted lines). For $T=33.0$ K pairs of lines are labeled with the same symbol. The lines labeled with * and ○ correspond to the Rb(1) site.

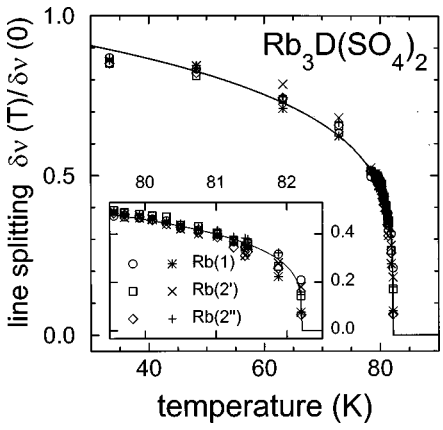

FIG. 8. Normalized line splitting as a function of temperature determined from the data presented in Fig. 7. The solid line represents a fit using a power law with $\delta\nu\propto(T-T_N)^{\beta}$ and $\beta=0.21\pm0.03$. The inset shows an enlarged view near the transition temperature.

As Fig. 6 shows, the quadrupole coupling at the Rb(2) site turned out to be temperature independent, with $\nu_Q=(3.83\pm0.1)$ MHz. However, for the coupling constant at the Rb(1) site a pronounced temperature dependence shows up above about 100 K. Here the variation in ν_Q is much stronger than expected from effects of thermal lattice expansion.[19] It should be noted however, that strongly temperature dependent coupling constants are also known from the ^{75}As resonances measured in the paraelectric phases of ammonium- or alkali-dihydrogen-arsenates.[20]

Since $\nu_Q(T)$ changes slope in the vicinity of the antiferroelectric phase transition temperature one might think that this effect is associated with the electrical ordering process. In order to test this notion we have also taken spectra of fully protonated samples which show no phase transition below room temperature. A comparison of Figs. 5(a) and 5(b) reveals that the temperature evolution of the spectra of $Rb_3H(SO_4)_2$ and of $Rb_3D(SO_4)_2$ is very similar. The temperature dependence of ν_Q as obtained from the simulation analysis and shown in Fig. 6 confirms this impression. This means that the magnitude of the quadrupolar coupling and hence the powder spectra of the deuterated sample are surprisingly little affected by the antiferroelectric phase transition. Therefore in order to investigate the phase transition itself single crystal studies are required.

C. Antiferroelectric phase transition

Single crystal spectra of $Rb_3D(SO_4)_2$ are shown in Fig. 7 for several temperatures near and below the paraelectric to antiferroelectric phase transition ($T_N=82$ K). Upon approaching T_N from above the resonance lines first broaden somewhat and then split into a number of (partially overlapping) components. At low temperatures (e.g., at 48.3 K) twelve peaks are clearly resolved, providing evidence for the quadrupling of the unit cell. The implications of these findings for the space group of the low temperature phase have been discussed elsewhere.[10]

In order to describe the spectra in the entire temperature range we have fitted them with a superposition of twelve Gaussian profiles which all exhibited the same width and integrated area. The results of these fits are shown as dashed lines in Fig. 7 and are seen to provide a good description of the data. The fitting parameters are presented in Figs. 8 and 9. The line splitting of each pair of lines (as marked by the pairs of symbols in Fig. 7) is seen to increase strongly below the antiferroelectric phase transition temperature. Furthermore, Fig. 8 documents that the splitting of each pair of lines as normalized to its value for $T\rightarrow0$ is the same within experimental error. Therefore, $\delta\nu(T)/\delta\nu(0)$ provides a good measure of the order parameter of the low temperature phase. The normalized splitting for all lines could be fitted using the same power law $\delta\nu\propto(T-T_N)^{\beta}$ where β is the order parameter exponent. Independent of the temperature range for which the fit was carried out we find $T_N=(82.1\pm0.1)$ K and $\beta=0.21\pm0.03$. A similar exponent ($\beta=0.25$) was reported

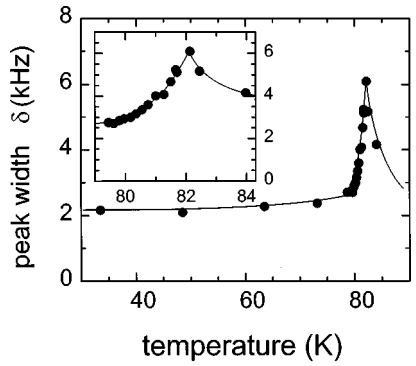

FIG. 9. Linewidths δ as determined from the data presented in Fig. 7. The inset gives an enlarged view of the line broadening showing up near T_N. The solid lines are drawn to guide the eye.

from a Raman scattering study on $K_3D(SO_4)_2$.[21] For a phase transition in the vicinity of a tricritical point a mean field exponent of $\beta=0.25$ is expected, but it is noted that similar exponents have also been determined on the basis of mean field models incorporating strongly anharmonic potentials.[22]

The inset of Fig. 8 reveals that close to T_N the scaled line splittings differ somewhat. The reason for this observation can be related to the fact that, in the vicinity of the transition temperature, the lines broaden. This hampers a precise determination of the magnitude of splitting.

The full width at half maximum, δ, of the resonance lines, as determined from the data presented in Fig. 7, is shown in Fig. 9. In the vicinity of the antiferroelectric transition $\delta(T)$ is reminiscent of the temperature dependence of the spin-lattice relaxation rate, $1/T_1$.[10] Near T_N, $1/T_1$ is strongly enhanced due to the slowing down of a soft mode which drives the antiferroelectric phase transition. From T_1 measurements at several Larmor frequencies it was suggested that the soft mode remains fast on the time scale set by the Larmor frequency.[10] In analogy with these findings we interpret the increase in linewidth seen for $T\approx T_N$ in Fig. 9 as a signature of the soft mode behavior.

Finally we would like to comment on the fact that the variation of the line splittings seen in Fig. 7 obviously do not reflect changes in the magnitude of the quadrupolar coupling constants (cf. Fig. 6). This means that below T_N the line shifts seen in the single crystal spectra (Fig. 7) correspond to variations in the *orientations* of the EFG tensors. Since the changes in the resonance frequencies are small ($<$70 kHz, cf. Fig. 7) as compared to ν_Q, via Eq. (3) the order parameter can be expected to be directly proportional to the displacements of the ions which contribute to the EFG at the Rb sites.

After the present article was submitted we became aware of an NMR study on $Rb_3H(SO_4)_2$ and $Rb_3D(SO_4)_2$ by Dolinsek *et al.*[23]

V. CONCLUSIONS

Single crystals as well as powders of $Rb_3D(SO_4)_2$ were studied using ^{87}Rb-NMR. At room temperature we have determined the magnitudes and orientations of the EFG tensors. These were found to be fully compatible with the symmetry of the monoclinic $A2/a$ ($Z=4$) structure indicated by x-ray scattering. The symmetric Rb(1) unit is characterized by an axially symmetric EFG tensor and a relatively large and strongly temperature dependent quadrupole coupling $\nu_Q(T)$. The eight crystallographically equivalent but magnetically pairwise inequivalent Rb(2) sites exhibit a temperature independent coupling constant ($\nu_Q=3.8$ MHz) and asymmetry parameter ($\eta=0.45$). For $Rb_3D(SO_4)_2$ $\nu_Q(T)$ changes slope in the vicinity of the antiferroelectric phase transition temperature ($T_N=82$ K). However, as a surprising result we find a practically identical temperature dependence of $\nu_Q(T)$ for the fully protonated compound, $Rb_3H(SO_4)_2$, which shows no electrical order at low temperatures.

Since below T_N the quadrupolar couplings do not change appreciably, the temperature dependence of the second order shifts of the central Rb transitions as seen in the single crystal spectra obviously indicate that the EFG tensors become tilted with respect to their high temperature orientations. The smooth evolution of the line positions or line splittings observed below T_N indicates that this tilt increases in a fashion that is expected for a second order phase transition.

The antiferroelectric phase transition in $Rb_3D(SO_4)_2$ is driven by a soft mode. This mode remains always fast on the time scale set by the Larmor frequency and leads to a sharp increase of the spin-lattice relaxation rate near T_N.[10] It also gives rise to the increase of the linewidth as observed in the single crystal spectra near the antiferroelectric transition temperature.

ACKNOWLEDGMENT

This project was supported by the Deutsche Forschungsgemeinschaft, Grant No. Bo1301/2.

*Permanent address: Institut für Festkörperphysik, Technische Universität, D-64289 Darmstadt, Germany.

[1] R. Blinc and B. Žekš, *Soft Modes in Ferroelectrics and Antiferroelectrics* (North-Holland, Amsterdam, 1974); R. Blinc and B. Žekš, Ferroelectrics **72**, 193 (1987).

[2] A. Bussmann-Holder and K. H. Michel, Phys. Rev. Lett. **80**, 2173 (1998).

[3] K. Gesi, J. Phys. Soc. Jpn. **61**, 162 (1992).

[4] For recent references see, e.g., C. Totsuji and T. Matsubara, Solid State Commun. **105**, 731 (1998); H. Sugimoto, J. Phys.: Condens. Matter **10**, 1237 (1998).

[5] M. Ichikawa, T. Gustafsson, and I. Olovsson, Solid State Commun. **87**, 349 (1993).

[6] Y. Moritomo, Y. Tokura, N. Nagaosa, T. Suzuki, and K. Kumagai, Phys. Rev. Lett. **71**, 2833 (1993).

[7] R. J. Nelmes, J. Phys. C **21**, L881 (1988).

[8] S. Ikeda and Y. Yamada, Physica B **213&214**, 652 (1995).

[9] S. Takeda, F. Kondoh, N. Najamura, and K. Yamaguchi, Physica B **226**, 157 (1996).

[10] A. Titze, G. Hinze, and R. Böhmer, Phys. Rev. B **57**, R666 (1998).

[11] S. Fortier, M. E. Fraser, and R. D. Heyding, Acta Crystallogr., Sect. C: Cryst. Struct. Commun. **41**, 1139 (1985).

[12] A. Abragam, *The Principles of Nuclear Magnetism* (Oxford University Press, Oxford, 1961).

[13] G. M. Volkoff, Can. J. Phys. **31**, 820 (1953).

[14] O. Liechti and R. Kind, J. Magn. Reson. **85**, 480 (1989).

[15] C. P. Slichter, *Principles of Magnetic Resonance*, 3rd ed. (Springer, Berlin, 1990).

[16] D. Freude and J. Haase, *NMR-Basic Principles and Progress* (Springer, Berlin, 1993), Vol. 29.

[17] Very recently the possibility has been raised by T. Gustafsson, M. Ichikawa, and I. Olovsson, J. Korean Phys. Soc. **32**, S199 (1998), that $Rb_3H(SeO_4)_2$ at room temperature exhibits the $A2$ structure. For this symmetry the expected number of resonance peaks is larger than experimentally observed. This implies that either the symmetry departure is below our detection limit or that the symmetries of $Rb_3H(SeO_4)_2$ and $Rb_3H(SO_4)_2$ differ.

[18] The asymmetry in the intensity of the outer [Rb(1)] resonances seen at low temperatures is due to the combined effects of finite pulse lengths and limited bandwidth of the resonance circuit.

[19] Below room temperature the total thermal contraction of $Rb_3D(SO_4)_2$ amounts to about 2%. [Y. Noda, Y. Watanabe, H. Kasatani, H. Terauchi, and K. Gesi, J. Phys. Soc. Jpn. **60**, 1972 (1991)]. Thus from the considerations presented below Eq. (3) it follows that the corresponding variation of ν_Q should not be larger than about 5%. Y. Noda, Y. Watanabe, and H. Terauchi, *ibid.* **61**, 905 (1992), who investigated $K_3H(SO_4)_2$ using x-ray scattering, report that while K(2) remains centered on its symmetry position, the position of K(1) exhibits a weak linear temperature dependence for $T>100$ K. For $T<100$ K the position exhibits a much weaker temperature dependence.

[20] J. L. Bjorkstam, Adv. Magn. Reson. **7**, 1 (1974).

[21] P. Kaung, M. Kasahara, and T. Yagi, J. Phys. Soc. Jpn. **65**, 1114 (1996).

[22] S. Radescu, I. Etxebarria, and J. M. Pérez-Mato, J. Phys.: Condens. Matter **7**, 585 (1995).

[23] J. Dolinšek, U. Mikac, J. E. Javoršek, G. Lahajnar, R. Blinc, and L. F. Kirpichnikova, Phys. Rev. B **58**, 8445 (1998).